Shear behavior of FRP-UHPC composite beams enhanced by FRP shear key: Experimental study and theoretical analysis

Shear behavior of FRP-UHPC composite beams enhanced by FRP shear key: Experimental study and theoretical analysis

Zhiwen Zhang[1], Ashraf Ashour[2], Wenjie Ge[1]*

[1.] Department of Civil Engineering, Yangzhou University, Yangzhou 225127, China.

[2.] Faculty of Engineering and Digital Technologies, University of Bradford, Bradford, BD71DP, UK.

** Corresponding author. Email address: gewj@yzu.edu.cn (Wenjie Ge).*

Abstract: To investigate the shear behavior of FRP (fiber reinforced polymers)-UHPC (ultra-high performance concrete) composite beams, four-point bending tests were conducted on seven FRP-UHPC specimens and two FRP-NSC (normal strength concrete) specimens, having different width and depth of concrete flange as well as FRP shear key (FSK) spacing. The slip between FRP profiles and concrete flange was controlled by employing FSK and epoxy resin bonded hybrid connection. The failure pattern, load-deflection/strain curves, and sliding response of composite beams were analyzed to study the influence of concrete type, FSK spacing, width and thickness of concrete slab. The results indicate that FRP-UHPC composite beams exhibited shear failure, while FRP-NSC composite beams experienced bending-shear failure. The composite beams demonstrated shear-lag effect, which became more pronounced with the increasing of the concrete slab width. The use of UHPC, reducing FSK spacing, and increasing the size of cross-section of concrete flange can effectively enhance the shear performance and reduce interface sliding. Formulae were developed to predict the shear capacity and deflection, considering shear deformation. The results predicted by the formulae developed match well with the experimental results.

Keywords: composite beam; shear performance; FRP profile; UHPC; FRP shear key

1 Introduction

Reinforced concrete (RC) structures are suffering from serious corrosion problems, which not only significantly reduce their expected lifespan but also lead to increases in maintenance expenses [1]. Fiber-reinforced polymers (FRP), renowned for its exceptional physical and chemical stability [2], effectively satisfies structural load requirements while exhibiting outstanding corrosion resistance [3], leading to its growing application in structural engineering [4]. By reinforcing the tension area with FRP profiles, the FRP-concrete composite structures not only mitigate the low stiffness of the individual FRP component but also enhances the overall structural stiffness and durability [5-6]. FRP-concrete composite structures, being both economical and practical compared to pure-FRP counterparts, combine the excellent corrosion resistance and high tensile strength of FRP while possessing the good compressive strength and low cost of concrete [7-8]. The load capacity of FRP-concrete composite beams increased by approximately 50%, while the self-weight decreased by around 50% [9] when compared with equivalent RC beams.

Despite the numerous advantages associated with FRP-concrete composite structures, they face a multitude of challenges. Although FRP-concrete composite beams adhere to the overarching concept of steel-concrete composite beams, there is a significant disparity in the shear strength exhibited by pultruded FRP compared to steel profiles. Based on the single-fiber failure model, Wang et al. [10] conducted an analysis on the failure patterns of FRP-concrete composite beams in terms of bending and shear. By testing eight low shear force connection performance composite beams, Neagoe et al. [11] developed and validated the FRP-concrete composite beam design method that considered shear effects. Based on the bending tests, Zou et al. [12] demonstrated that the strength of the resin and interfacial bond significantly influence the shear performance of FRP profiles. Besides, the ply angle of fibers also plays a role in determining shear strength. Specifically, FRP profiles with a 0° ply angle (produced through pultrusion process) exhibited lower shear strength compared to those with a 45° ply angle, which showed higher shear strength. However, considering the trade-off between manufacturing cost and advantages associated with pultrusion process, currently, profiles produced with a 0° ply angle are widely utilized in engineering applications. This characteristic makes FRP-concrete composite beams prone to shear failure during service, especially at the junction of the FRP web or web-top flange [13].

Effective mitigation of bond failure between FRP and concrete can be achieved through the development of efficient shear connector [14]. For FRP-concrete composite beam, the FRP and concrete are joined together by interfacial shear connection such as perforated FRP rib, epoxy adhesive, steel/FRP bolts or steel/FRP shear key [9]. Zhang et al. [15] tested FRP box-concrete composite beams with different interface treatments. The experimental results demonstrated that the FRP-concrete composite beam with a box section exhibited enhanced load-bearing capacity and flexural stiffness in comparison to the pure-FRP box beam, despite both beams exhibiting shear failure of the FRP web. They also confirmed that the combination of using FRP shear key (FSK) and bonded interfaces exhibited the best anti-slip performance. Thus, the design process for FRP-concrete composite sections is typically governed by shear capacity, highlighting the crucial importance of investigating the shear performance.

The recently developed cement-based composite material, UHPC [16], exhibits exceptional durability and ultra-high strength [17]. Research studies [18-19] have demonstrated that the rational utilization of FRP's excellent mechanical properties in conjunction with UHPC can enhance the loading and durability capacities of structures while reducing the potential risk of microcracks expanding within structures. By combining FRP and UHPC, the performance shortcomings of traditional RC in extreme environments can be mitigated, enabling bridge structures to achieve higher efficiency, cost-effectiveness, and sustainability.

Currently, there are few studies focusing on the factors influencing the shear performance of FRP-UHPC composite beams. The applicability of existing design theories and specifications for FRP-NSC composite structures to FRP-UHPC composite structures has not been verified. In addition, the anisotropic characteristics of FRP make the failure patterns of composite beams more diverse and complex [20], posing challenges in the derivation of design theories and universally accepted specifications for FRP-UHPC composite structures. Therefore, it is necessary to conduct systematic experimental and theoretical research to explore the shear behavior of FRP-UHPC composite beams with a single web.

In this paper, the FRP-UHPC composite beams were subjected to four-point bending tests by varying the concrete type, FSK spacing, concrete slab width, and thickness as the main parameter variables. According to the findings presented by Zhang et al. [15], a hybrid treatment of FSK and epoxy resin was applied to the interface between concrete and FRP top flange in order to further mitigate interfacial slip-induced failure. Based on the tested results, including failure pattern, load-displacement response, strain response, and slip response, the mechanism of FRP-UHPC composite beams enhanced by FSKs under shear failure was thoroughly investigated. Additionally, the formulae for shear bearing capacity and deflection considering shear deformation were derived based on appropriate assumptions. The output results can provide a valuable technological reference for the design of FRP-UHPC composite beams.

2 Experimental programs

The FRP-UHPC composite beams enhanced by FSK were designed and fabricated at a 1/2 scale, as show in Fig. 1. The total length of specimens is 1800 mm, bending-shear span is 600 mm, and pure bending span is 400 mm. Specimen S1 has FRP profiles with dimensions of 180 × 100 × 10 × 10 mm ($h_{\mathrm{fw}} \times b_{\mathrm{fw}} \times t_{\mathrm{fw}} \times t_{\mathrm{fw}}$) and UHPC slab with cross-sectional dimension of 200 × 60 mm ($b_{\mathrm{c}} \times t_{\mathrm{c}}$), was taken as control specimen. The dimensions of FSK are 3 × 40 × 40 mm ($t_{\mathrm{s}} \times b_{\mathrm{s}} \times h_{\mathrm{s}}$) and the spacing d_{f} is 200 mm. To study the influence of FSK spacing on the shear performance of FRP-UHPC composite beams, the FSK spacing of beams S4, S1 and S5 is set to 100 mm, 200 mm and 300 mm, respectively. The specific layout details are shown in Fig. 1(d), (e) and (f). A hybrid connection of epoxy resin and FSK was used for the composite interfaces of all specimens [15]. First, the surfaces of the bottom of FSK and the FRP upper flange were roughened by a grinding machine, then cleaned by industrial-grade alcohol. Second, the FSKs were adhered onto the upper flange surface of the FRP profile by modified epoxy resin (E-44). After securely attached, epoxy resin was brushed onto the surface of upper flange, and concrete was directly poured into the formwork. After 28 days of natural curing, formwork was removed.

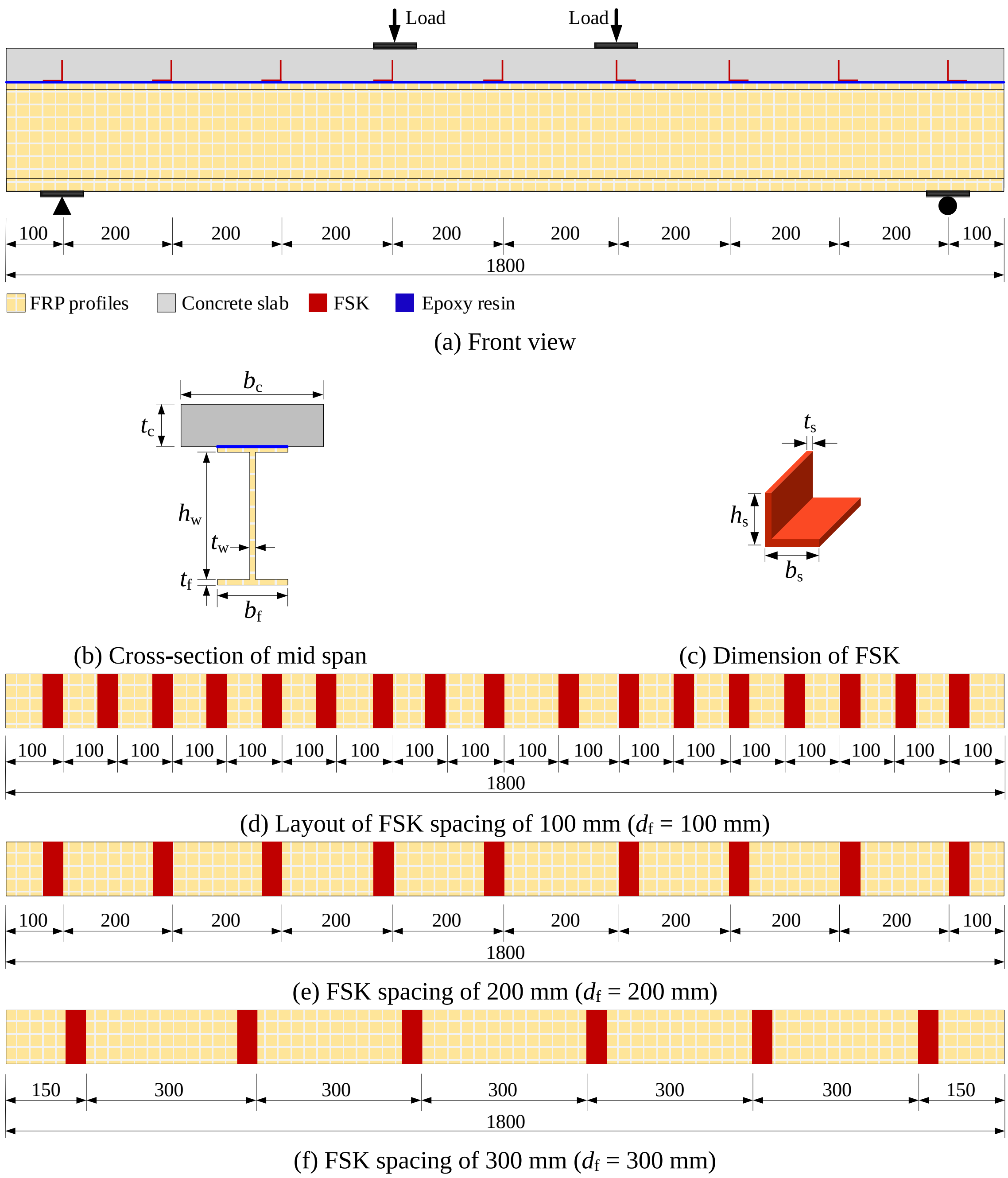

Fig. 1. Dimension of FRP-UHPC composite beams enhanced by FSK (unit: mm).

Tab. 1. Parameters of specimens designed.

No.	Type of concrete	t_c (mm)	b_c (mm)	d_f (mm)
S1	UHPC	60	200	200
S2	C40	60	200	200
S3	C60	60	200	200
S4	UHPC	60	200	100
S5	UHPC	60	200	300
S6	UHPC	60	100	200
S7	UHPC	60	300	200
S8	UHPC	80	200	200
S9	UHPC	100	200	200

2.1 Mechanical properties of materials

Table 2 delineates the mixture compositions for NSC and UHPC, adhering to the specifications outlined in Chinese standards JGJ 55-2019 [21] and GB/T 31387-2015 [22], respectively. Both NSC and UHPC formulations feature manufactured sand characterized by an average particle size of 0.5 mm and employ Portland cement, with NSC utilizing P.II 42.5 grade and UHPC employing P.II 52.5 grade cement. NSC incorporates coarse aggregates ranging from 5 to 20 mm in particle size. The composition of UHPC includes active mineral admixtures such as 400 mesh silica fumes (the number of holes in the screen per inch is 400 particles, and the particle diameter is about 37 microns), grade II fly ash, and grade S95 slag powder. Additionally, straight copper-plated steel fibers, possessing a tensile strength of 2850 MPa and dimensions of 13.0 mm in length and 0.22 mm in diameter, are integrated into the UHPC mixture. Mixing water sourced locally and a polycarboxylate superplasticizer with a solid content of 20% and a water reduction rate of 32% are employed in both formulations.

Tab. 2 Mixture proportions by weight of NSC and UHPC.

No.	Cement	Sand	Stone	Slag powder	Silica fume	Fly ash	ρ_s (%)	Superplasticizer (%)	w/b
C40	1.0	1.64	2.67	/	/	/	/	1.05	0.42
C50	1.0	1.11	2.59	/	/	/	/	1.2	0.32
UHPC	0.55	1.2	/	0.1	0.25	0.1	1.0	1.5	0.19

Note: ρ_s is the volume fraction of steel fiber, and w/b is the water-binder ratio.

According to Chinese codes GB/T 50081-2019 [23] and T/CBMF 37-2018, T/CCPA 7-2018 [24], respectively, three dumbbell-shaped concrete specimens for tension test and three cubic concrete specimens for compression test (100 × 100 × 100 mm) were prepared under the same condition as the beam specimens. Table 3 lists the mechanical properties of UHPC and NSC, where f_{cu} is the cubic compressive strength tested, E_c, f_c and f_t are the calculated modulus of elasticity, compressive and tensile strength, respectively [25].

Tab. 3 Mechanical performance of NSC and UHPC.

No.	f_{cu} (MPa)	f_c (MPa)	f_t (MPa)	E_c (GPa)
C40	45.8	34.8	2.8	33.8
C50	57.5	43.7	3.2	35.7
UHPC	106.4	93.6	7.9	43.2

The FRP profiles with an apparent density of 1920 kg/m^3 were manufactured by using the pultrusion process method (glass fiber and unsaturated polyester resin). Symmetric and balanced laying plans were adopted for the fibers at the flange and web. Accordance to the ASTM D3039/D3039M-14 [26] and GB/T 1448-2005 [27], material performance tests were carried out on the FRP profiles. The test results show that the uniaxial tensile and compressive strength are 375 MPa and 328 MPa, respectively, while the tensile and compressive modulus of elasticity are 33.8 and 30.4

GPa, respectively. The shear performance data was acquired from manufacturer tests conducted in accordance with ASTM D3518/D3518M-18 [28]. The results indicate that the in-plane shear strength along the fiber direction is 35.8 MPa, while the corresponding shear modulus is measured to be 3.7 GPa.

According to the testing report offered by the manufacturer, the epoxy resin has a tensile strength of 40.5 MPa, shear strength of 12.7 MPa, a modulus of elasticity of 3.4 GPa, its bond strength with concrete (cohesive failure) is 3.7 MPa and elongation is 2.3%. It has a curing time of 4 to 6 hours, and a temperature resistance of -60 ℃ ~ 120 ℃.

2.2 Test setup and measurements

Figure 2 exhibits the experimental configuration, loading apparatus, and measurement layout utilized in the four-point flexural testing procedure. The vertical deformation was monitored by displacement gauges placed at the bottom of the specimen and two supports. Dial gauges were used to assess the longitudinal slip between the concrete slab and FRP profiles. The recorded end slip of the beam specimen was determined by calculating the differential longitudinal displacements between the top flange of the FRP profile and the concrete slab. The measurement of strain distribution was achieved by bonding strain gauges on both the concrete slab and FRP profiles of mid-span sections. In order to evaluate web shear strain within the shear span, three rows of three-directional rosette gauges were uniformly placed at sections located 200 mm and 400 mm away from the support. After polishing the paste position, it is recommended to thoroughly clean it with alcohol before attaching the strain gauge. To mitigate any potential impact of hydration heat generated by UHPC during the hydration process on the electric couples of the strain gauge, all surfaces of the strain gauge are coated with epoxy resin adhesive. Furthermore, prior to conducting bending tests, it is essential to meticulously verify the validity of all measuring points in order to prevent data errors caused by strain damage. Load, strain, and displacement were captured throughout the loading process using a TDS 540 data acquisition instrument. Additionally, four wooden pads with dimensions of 100 × 45 × 200 mm (width × thickness × height) were positioned at the bottom support to mitigate failure resulting from localized stress concentration on the bottom flange of the FRP profiles.

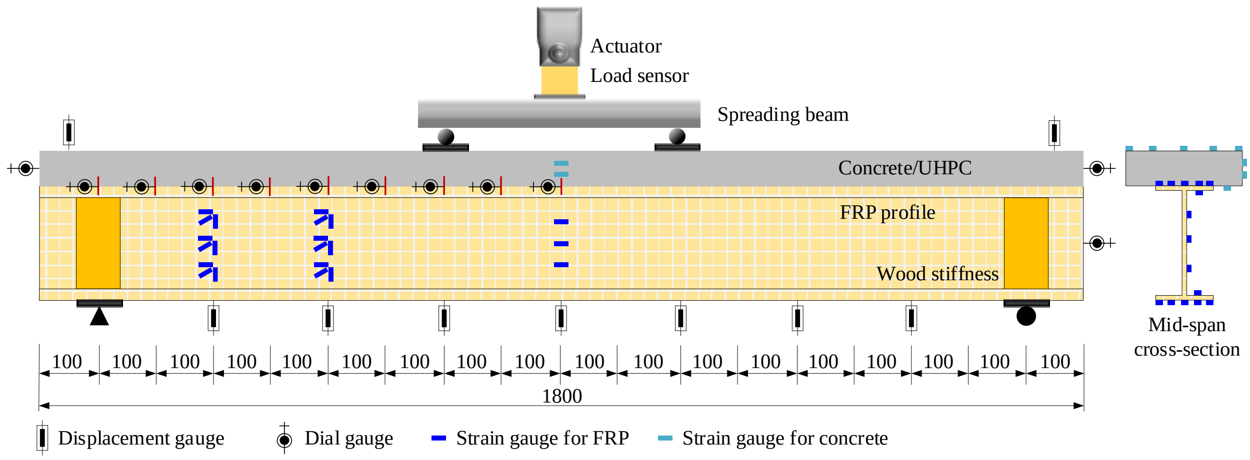

Fig. 2. Test setup (unit: mm).

3 Experimental results

3.1 Failure modes

The general failure patterns of all specimens are illustrated in Figure 3, and these patterns have been summarized in Table 4. All specimens cracked at the lower edge of concrete slab at the mid span during the initial bending stage, accompanied with slight noises, and significant increase of the end slips. With the increase of load, tearing occurred at the web-flange connections at the ends of beams (Fig. 3a). Blisters appeared on the matrix of FRP profiles, and the interlayer adhesive layers began to delaminate. Due to the low compressive strength of NSC, the top of concrete slab at mid-span crushed (Fig. 3b), and specimens S2 and S3 (FRP-NSC composite beams) reached ultimate failure, with bottom cracks extending near the loading points. The shear failure at the web-flange connections gradually worsened and spread from the ends to the loading points. Besides, when specimen S2 failed due to severe tearing of the web, the bonding of the interface weakened, and delamination occurred between the top flange of FRP profile and end concrete slab (Fig. 3d). As a result, the FRP-NSC composite beam experienced a cooperative failure involving both bending and shear. The concrete slabs in FRP-UHPC composite beams showed diagonal cracks in the shear span, extended from shear span to pure flexural span (Fig. 3c). When the interlayer shear at the web-flange connection extended to the pure bending span, the end web suddenly cracked, and the composite beam collapsed, gradually recovering after unloading. Therefore, the FRP-UHPC composite beam exhibited mainly shear failure. The development of internal microcracks and macroscopic cracks were effectively restricted by the steel fibers distributed in UHPC matrix. The crack widths of FRP-UHPC composite beams are smaller and denser than those of FRP-NSC composite beams. Steel fibers slowly pulled out from the matrix before the failure of specimens, indicating the bridging effect of UHPC with random distributed steel fibers improved the deformation capacity and ductility of composite beams.

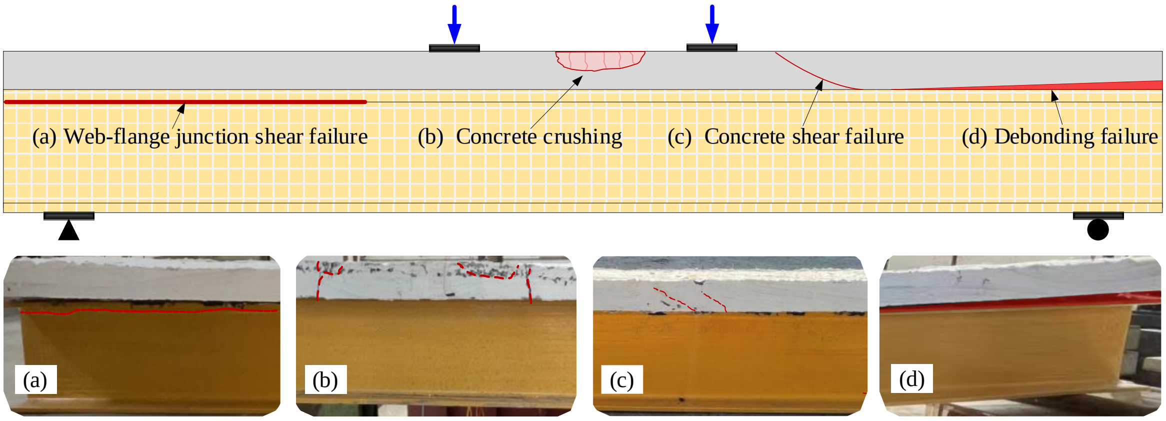

Fig. 3. General failure modes.

Tab. 4. Summarization of all the specimens' failure modes.

Failure mode	Specimen
Debonding failure	S2
Concrete compression failure	S2, S3
Concrete shear failure	S1, S4, S5, S6, S7
Web-flange junction shear failure	S1, S2, S3, S4, S5, S6, S7, S8, S9

3.2 Load response

3.2.1 Load-deflection curve

Figure 4 displays the load-deflection (P-δ) curves, and the comparison of test results of is listed in Table 5. P_{cr} and P_u are the cracking and ultimate load, respectively, δ_{cr} and δ_u are their corresponding deflections, respectively; s_l and s_r are the maximum slips at the left and right ends of concrete slab, respectively. According to the code JGJ 138-2016 [29], the deflection at the mid-span of the beam under serviceability limit state is considered as the deflection limit ($\delta_{limit} = 6$ mm), that is 1/300 of the total span. It can be observed that when the deflection reaches the deflection limit in such the state, the FRP-UHPC composite beam reinforced by FSKs still has a large load reserve. Thus, the FRP-UHPC composite beam with FSK meets the requirements for serviceability limit state.

As illustrated in Fig. 4, the load-deflection curves of both FRP-UHPC and FRP-NSC composite beams demonstrate elastic behavior till the cracking of concrete slab. After cracking, the load-deflection curves of FRP-UHPC composite beams maintain an almost linear progression until failure, whereas the curves for FRP-NSC composite specimens exhibit a nonlinear pattern. This difference in behavior can be attributed to the contrasting material performance between NSC and UHPC. In FRP-NSC composite beams, the bending process leads to a concrete crushing stage, followed by interlayer shear failure, primarily due to the lower strength of NSC compared to UHPC. Conversely, FRP-UHPC composite beams tend to develop small and dense shear cracks during bending, eventually leading to failure primarily due to shear at the web-flange connection. These distinct failure modes result in different characteristics during failure. When shear failure occurs, the FRP-NSC composite beams can exhibit pseudo-ductile behavior [30], allowing some deformation and load redistribution.

However, FRP-UHPC composite beams, with their higher strength and more rigid response, tend to fail in a more brittle pattern.

After comparing specimens S1, S2, and S4, it can be observed that the ultimate load of specimen S1 is enhanced by 15.1% and 11.3%, while the ultimate deflection is reduced by 3.6% and 1.3%, respectively, in comparison with S2 and S4. This suggests that the utilization of UHPC instead of NSC can enhance the shear performance of composite beams to a certain extent; however, it may expedite the shear failure of FRP profiles and diminish the deformation capacity of composite beams [31]. As the FSK spacing is reduced, the cracking and ultimate loads together with their respective corresponding deflections improved (Fig. 4b). This indicates that reducing the spacing of FSK can moderately improve the synergetic performance of FRP profiles and UHPC slab, thereby enhancing the shear contribution of UHPC slab [32]. As the thickness and width of concrete slab increase, the cracking and ultimate loads increase, while their respective corresponding deflections decrease (Fig. 4c and Fig. 4d). The bearing capacity of specimen with a slab width of 300 mm is improved by 2.1% and 6.0%, respectively, compared with those of specimens with slab widths of 200 and 100 mm. The load bearing capacity of the specimen with a slab thickness of 100 mm is improved by 15% and 29%, respectively, compared with counterparts having slab thickness of 80 and 60 mm. This finding illustrates that enlarging the slab thickness of specimen has a certain extent effect on its shear performance. This can be attributed to the ratio of shear span to depth decrease with the increase of concrete slab thickness, thereby enhancing the shear performance of specimen accordingly.

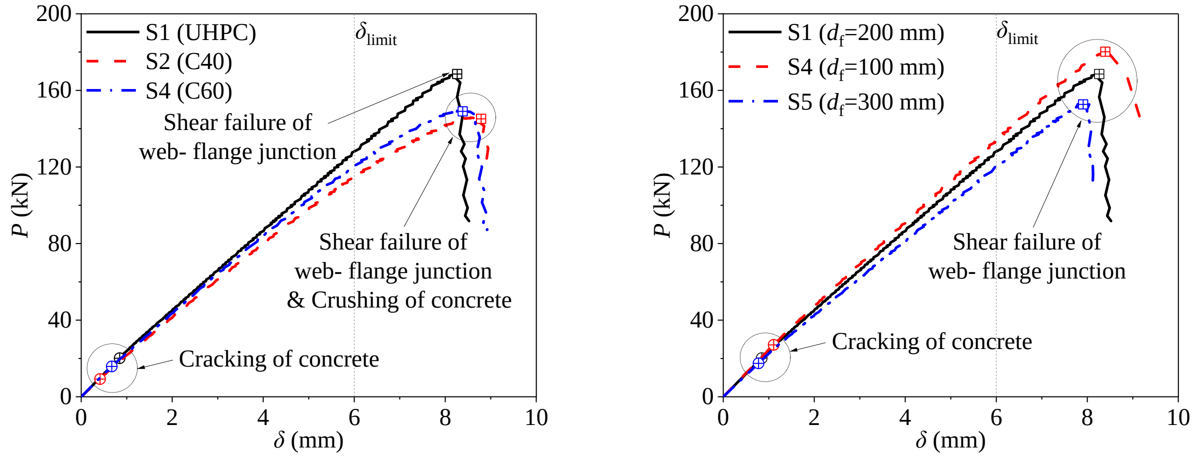

(a) Effect of concrete slab strength

(b) Effect of FSK spacing

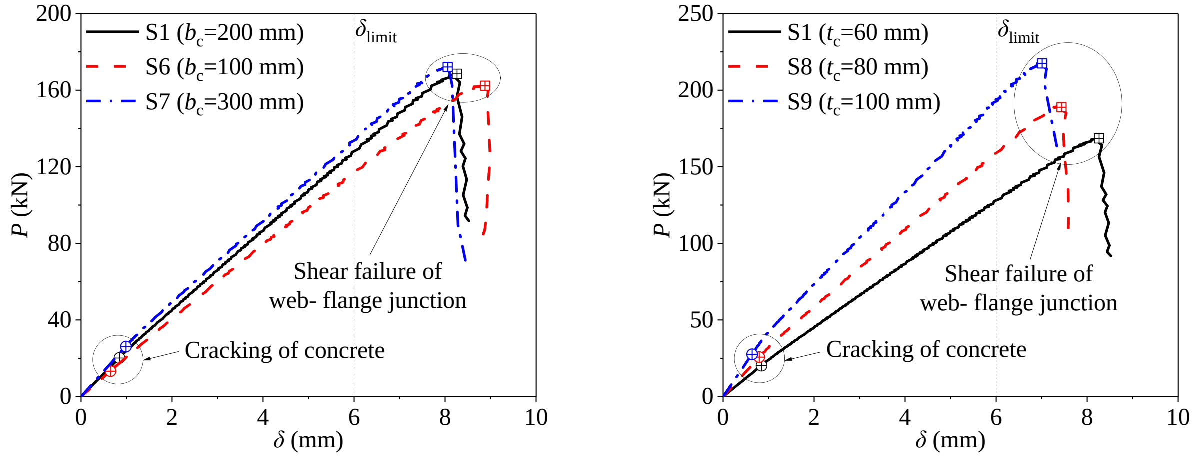

(c) Effect of concrete slab width

(d) Effect of concrete slab thickness

Fig. 4. Load-deflection curves.

Tab. 5. Characteristic load, deflection and failure mode.

No.	P_{cr} / kN	P_u / kN	δ_{cr} / mm	δ_u / mm	s_l / mm	s_r / mm	Failure pattern
S1	20.2	168	0.84	8.26	0.97	0.95	Shear
S2	9.33	146	0.41	8.56	1.72	1.76	Flexural & shear
S3	15.2	149	0.64	8.37	1.56	1.52	Flexural & shear
S4	25.8	180	1.05	8.39	0.79	0.80	Shear
S5	17.5	153	0.77	7.79	1.18	1.16	Shear
S6	19.6	162	0.96	8.88	0.64	0.66	Shear
S7	23.8	172	0.89	8.06	1.20	1.18	Shear
S8	25.8	190	0.79	7.39	1.27	1.29	Shear
S9	28.7	218	0.66	6.92	1.42	1.39	Shear

3.2.2 Stiffness degeneration

The stiffness degradation curves are illustrated in Fig. 5. Before the concrete cracking, the stiffness of all specimens almost unchanged. After concrete cracking, the interfacial slip gradually increases, resulting in nonlinear stiffness degradation. Before the concrete slab cracks, the initial stiffness of specimens with UHPC slab is slightly higher than that of specimen with C40 concrete slab, but close to that of specimen made of C60 slab. After reaching the serviceability limit state, the stiffness degradation of FRP-UHPC composite beams is more gradual, while that of FRP-NSC composite beams is more rapid. Therefore, although UHPC cannot obviously enhance the initial stiffness of composite beams, it can moderately delay the degradation of stiffness in composite beams. This can be attributed to the higher bonding strength of UHPC with FSK and FRP profiles than that of NSC, and the composite coefficient of FRP-UHPC composite beam is larger, resulting in improved overall integrity. The stiffness degradation of specimens with different spacing of FSK shows no significant difference. With the decrease of spacing of FSK, the stiffness increases. As the width and thickness of concrete slab increase, the stiffness also improves. Increasing the slab thickness exhibits a more significant influence on stiffness improvement, but the stiffness degradation rate also gradually increases. This is because as the section size of concrete slab increases, which accelerates the development of FRP profiles shear damage, leading to a significant improvement in interfacial bond slip and a decrement in composite coefficient.

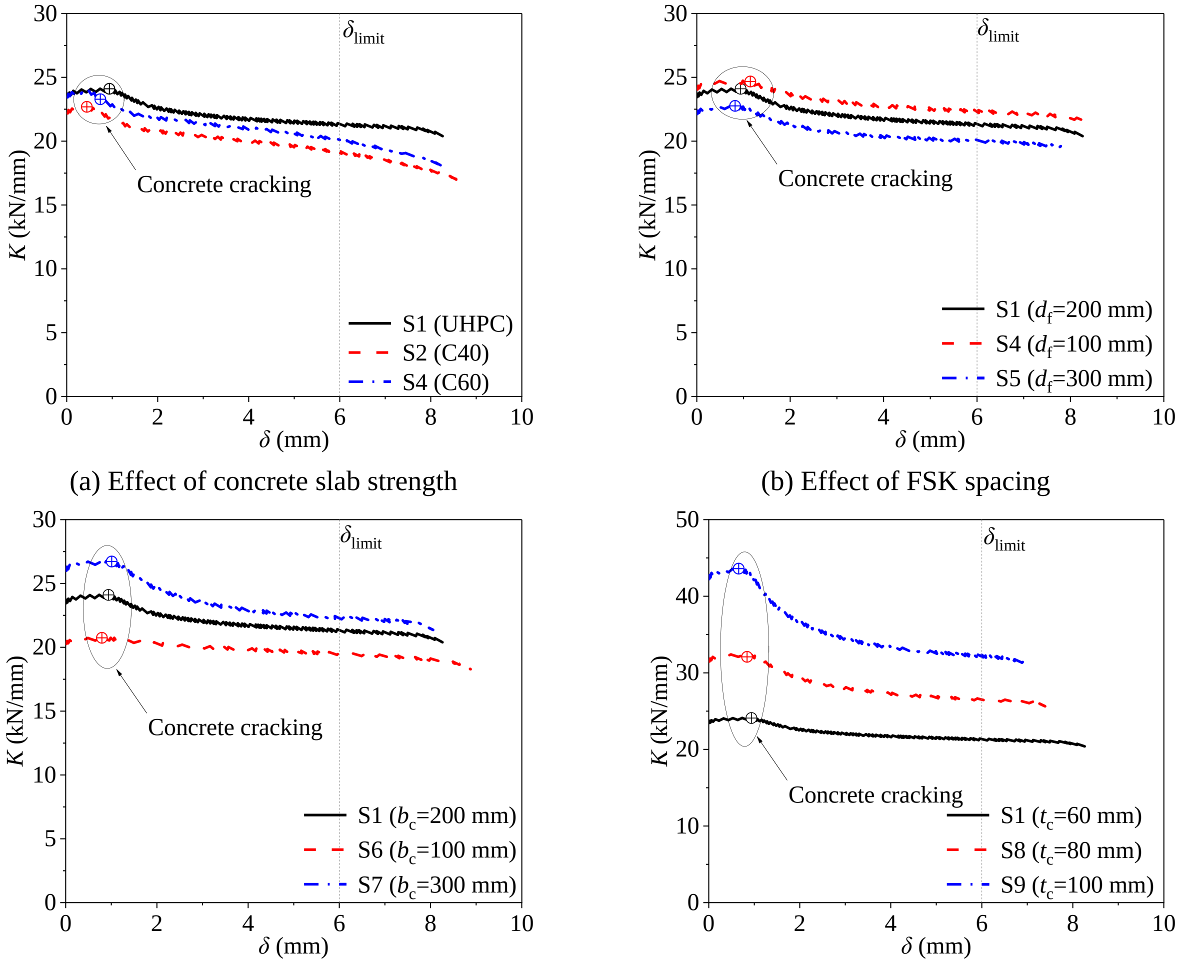

(a) Effect of concrete slab strength
(b) Effect of FSK spacing
(c) Effect of concrete slab width
(d) Effect of concrete slab thickness

Fig. 5. Stiffness degradation curves.

3.3 Strain response

3.3.1 Load-longitudinal strain curve

Figure 6 illustrates the load- longitudinal strain (P-ε) curve of the bottom of FRP profile and top of concrete slab at mid-span section. The load-strain curve also exhibits two obvious stages: elastic and elastoplastic stages. All FRP-UHPC composite beams exhibited approximately elastic behavior until failure, while FRP-NSC composite beams displayed non-linear behavior when the top concrete strain exceeded the peak compressive strain. As concrete at the measuring points of beam S2 and S3 (FRP-NSC composite beams) were crushed during the later loading stage, resulting in distorted data, only the curve before concrete failure is presented. The compressive strain in concrete for all FRP-UHPC composite beams did not reach the peak compressive strain of 0.0022, and the tensile strain of bottom FRP profiles is smaller than its longitudinal ultimate tensile strain of 0.0111, indicating the properties of UHPC and FRP profiles have not fully utilized and test specimens failed in shear. The

FRP profiles strain in some specimens decreased at the ultimate load due to the elastic-brittle property of FRP profiles, resulting in a rebound during unloading. Under the same loading, improving concrete strength, reducing the spacing of FSK and increasing the sectional dimension of concrete slab not only reduce strains in FRP profiles and concrete slab but also improve the stiffness of composite beams.

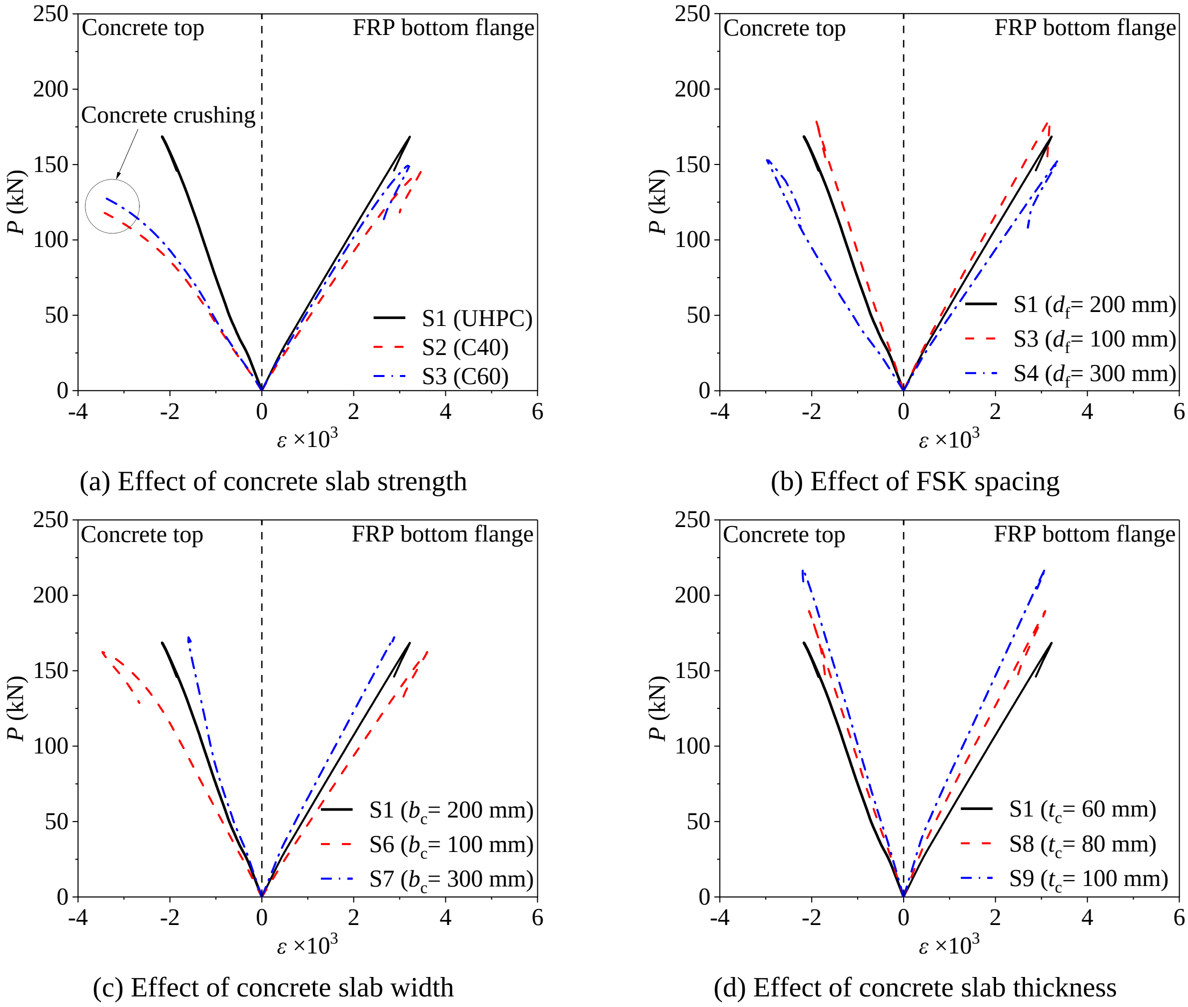

(a) Effect of concrete slab strength

(b) Effect of FSK spacing

(c) Effect of concrete slab width

(d) Effect of concrete slab thickness

Fig. 6. Load-longitudinal strain curves.

3.3.2 Load-shear strain curve

Assuming that the FRP web of composite beams is in a state of plane stress during the bending process, the shear strain γ_{xy} in FRP web could be calculated by using Eq. (1) [33], where, $\varepsilon_{0°}$, $\varepsilon_{45°}$, and $\varepsilon_{90°}$ represent the strains measured at 0°, 45° and 90° directions of the web in the shear span, as exhibited in Fig. 2.

$$\gamma_{xy} = \varepsilon_{0^\circ} + \varepsilon_{90^\circ} - 2\varepsilon_{45^\circ} \quad (1)$$

Figure 7 shows the load-shear strain (P-γ_{xy}) curves for the webs of all specimens. As all shear failures occurred at the connection between the flange and web of FRP profile, the shear strain at all measured points did not reach the ultimate shear strain of FRP web of 0.0097. With the increasing of concrete strength, the maximum shear strain at the measuring points also increases. Under the same load, the shear strain at measured point A in the web of FRP-UHPC composite beam is lower than that in FRP-NSC composite beam. Furthermore, it can be observed that the same outcome is achieved when comparing the shear strain of point B in both groups of composite beams. Therefore, UHPC can effectively enhance the shear stiffness of specimens, share the shear stress of FRP profiles, and improve the shear capacity of composite beams. In addition, reducing the spacing between FSKs and increasing the cross-section size of concrete slab also have similar effect. Among them, increasing the thickness of concrete slab results in the most significant influence on improving the shear performance.

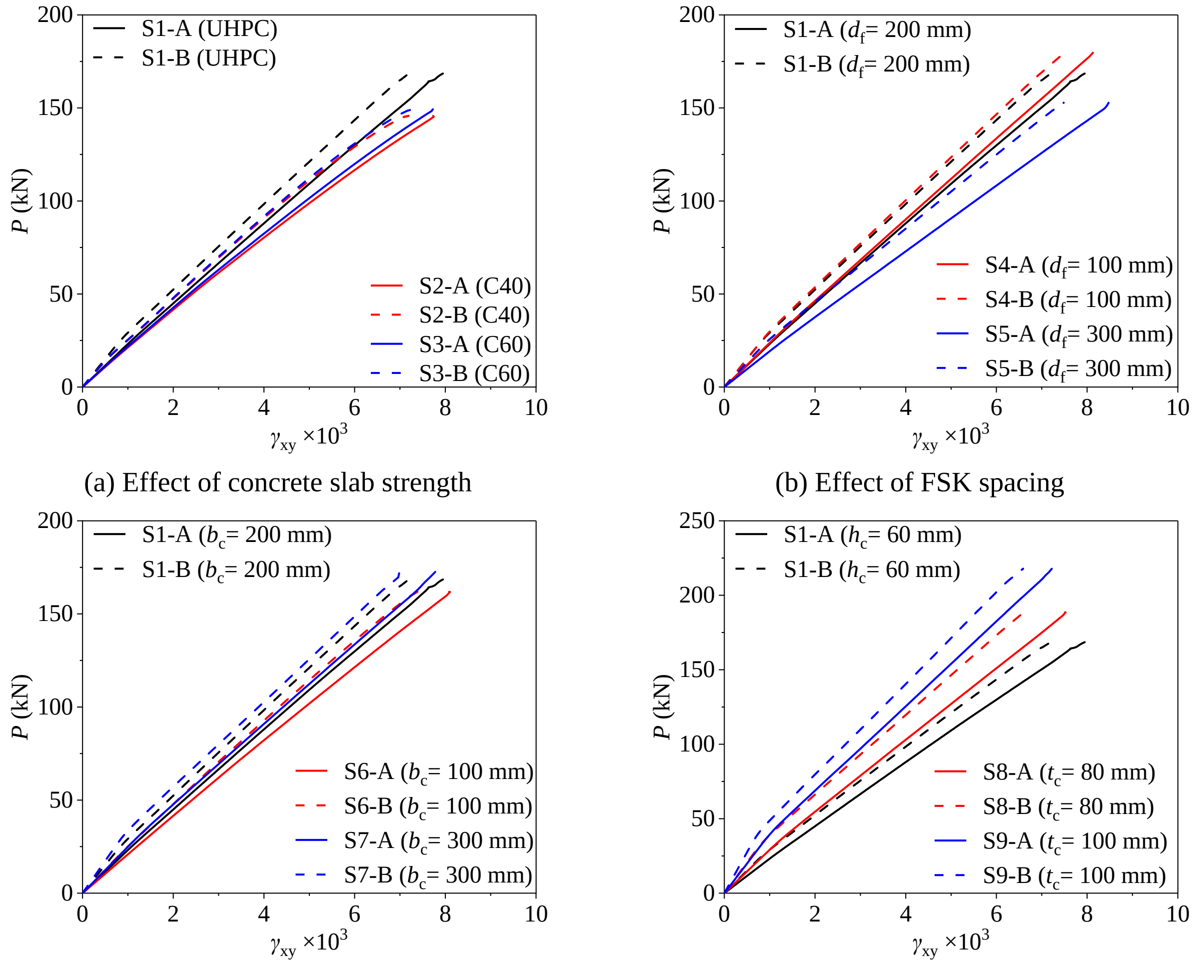

(a) Effect of concrete slab strength

(b) Effect of FSK spacing

(c) Effect of concrete slab width

(d) Effect of concrete slab thickness

Fig. 7. Load-shear strain curves.

3.3.3 Strain distribution along the sectional height direction

The mid-span sectional strain distribution curves along the height direction of all specimens are similar. Here, taking specimen S1 for an example, as illustrated in Fig. 8, the mid-span strain distribution along the height direction is approximately linear before the composite beam reaches failure, basically satisfying the plane section assumption. There was a significant interfacial slip between the concrete slab and FRP profile flange when the composite beam reached ultimate load.

As the interfacial slip severely weakened the composite action, stress redistribution occurred for both the FRP and concrete sections. Therefore, prior to the occurrence of interfacial slip, the mid-span strain of test specimens was in a coordinated and continuous state, representing one composite section. However, once interfacial slip occurred, the bottom of concrete slab began to sustain greater tensile strains, and the FRP flange started to bear greater compressive strains.

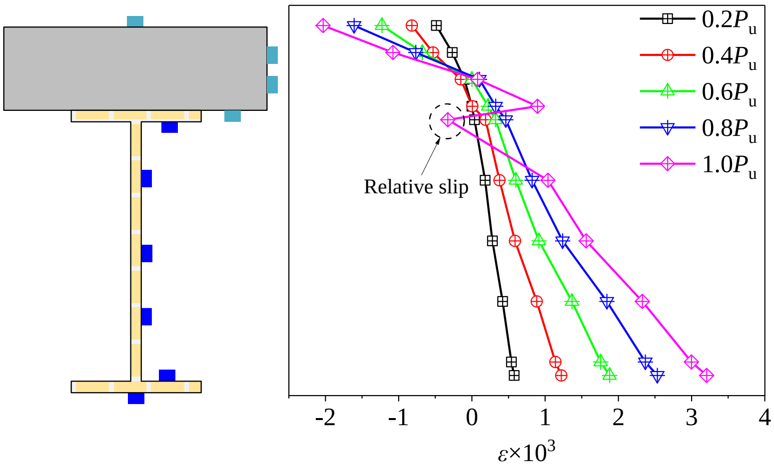

Fig. 8. Strain distributions along the sectional height direction.

3.3.4 Strain distributions along beam width direction

Figure 9 shows the mid-span transverse distribution curves of compressive strain on top of concrete slab for specimens S1, S6 and S7. In the elastic stage, the surface compressive strain of UHPC and the tensile strain of FRP bottom flange are uniformly distributed. But the strains mentioned above are no longer evenly distributed in elastic-plastic stage. Under different load levels, the strains at mid-axis are slightly greater than those at the ends, confirming the existence of shear lag effect in FRP-UHPC composite beams under bending moment [34]. By comparing specimens S1, S6, and S7, it can be found that the shear lag effect of specimens S1 (b_c = 200 mm) and S7 (b_c = 300 mm) are more significant than that of specimen S6 (b_c = 100 mm), indicating that with the increasing of concrete slab width, the shear lag effect is more pronounced. Therefore, the shear lag effect of composite beams cannot be ignored at higher loading.

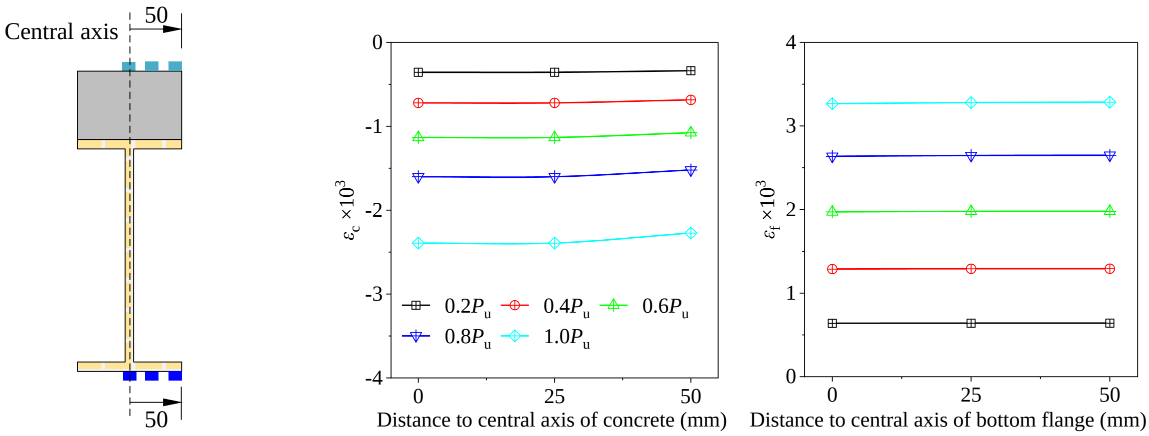

(a) b_c = 100 mm (S6)

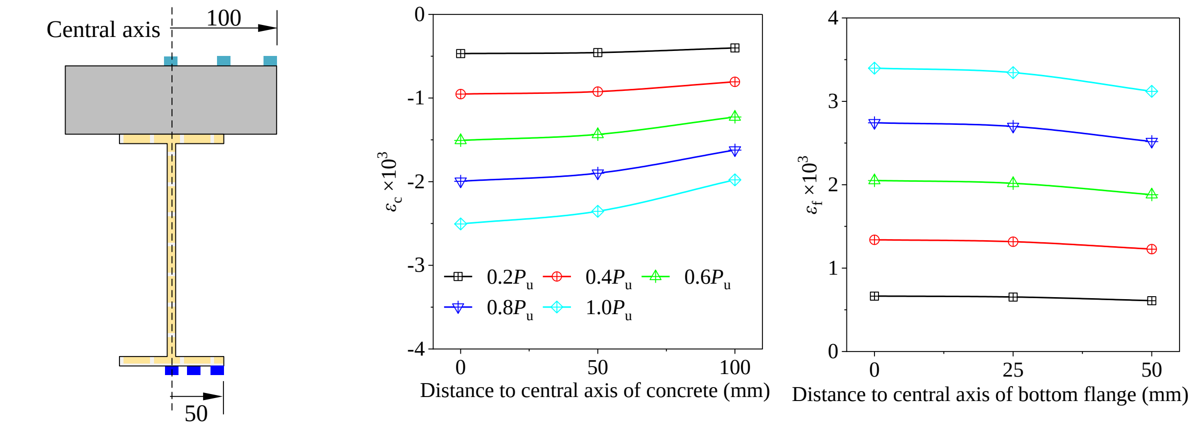

(b) b_c = 200 mm (S1)

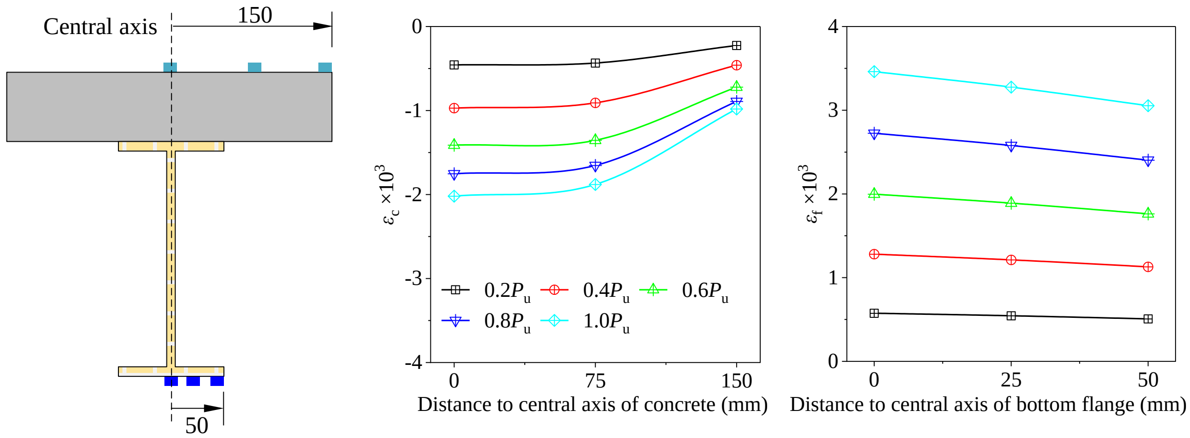

(c) b_c = 300 mm (S7)

Fig. 9. Mid-span sectional strain distributions along beam width direction.

3.3.5 Strain distribution of the bottom and top flanges along beam length direction

Figure 10 illustrates the longitudinal strain distributions along the bottom and top flanges of FRP section of specimen S1. The strain on the top flange of FRP remained positive, indicating the neutral axis keeps inside the concrete slab. The longitudinal strain distribution was basically synchronous with the bending moment distribution, agreeing with the principle of structural mechanics. The strains on the top and bottom flanges at mid-span are smaller than those at the loading points due to stress concentration. Under different loading levels, the strain distribution of bottom flange approximately follows a linear ascending or descending trend over the half span. The strain distribution of top flange is uneven, caused by shear-interface action of FSKs that are distributed at intervals. The interlayer shear failure occurred at the connection between the top flange and web when the composite beam reached its ultimate load, causes partial detachment and results in a sudden increase of strain in top flange.

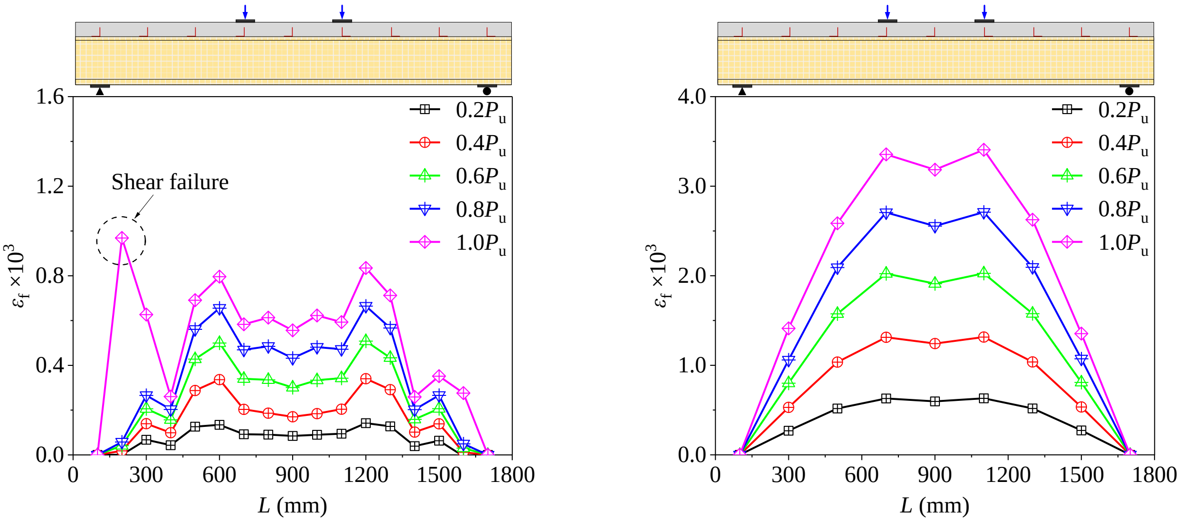

(a) Top flange (b) Bottom flange

Fig. 10. Strain distribution of the bottom and top flanges along the beam length (Beam S1).

3.4 Slip response

3.4.1 Relative slip along the length direction of beam

The distribution curve of the relative slip along the length direction of specimen S1 is illustrated in Fig. 11. Given the symmetical nature of the specimens, displacement gauges were installed only over half the beam's span. The slip remained relatively small and developed slowly during the elastic stage, but exhibited a marked increase as the beam transitioned to the elastic-plastic stage. Additionally, the slip was generally smaller within the pure flexural span but increased and exhibited a more uneven distribution in the flexural-shear span [35]. This phenomenon can be attributed to the localized anti-shear action of the FSKs, which effectively mitigate slip in spans incorporating FSKs compared to those without them. In summary, FSKs significantly enhance shear resistance at the interface, thereby improving overall structural integrity of composite beams.

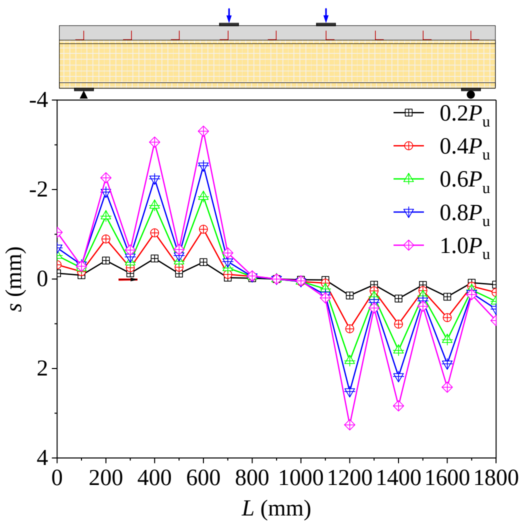

Fig. 11. Interfacial slip distribution along the length direction of specimen S1.

3.4.2 Deflection-slip curve

The vertical deflection-slip (δ-s) curves for all tested specimens is shown in Fig. 12. It is evident that for composite beams occurring the same deflection, the end slip in FRP-NSC specimens is greater than in FRP-UHPC specimens. Furthermore, the end slip tends to decrease as the strength of the NSC increases (Fig. 12a). This suggests that UHPC demonstrates superior bond performance with FRP, indicating stronger interface shear resistance at the FRP-UHPC composite interface compared to the FRP-NSC interface. According to the findings of Lu et al. [36], the enhanced tensile strength and crack resistance of UHPC contribute to its improved bonding performance with FRP. In terms of specimens with the same deflection, the maximum end slip was observed in the specimen having FSK spacing of 300 mm, while the specimen having FSK spacing of 200 mm showed a moderate level of end slip, and the specimen having FSK spacing of 100 mm exhibited the least end slip (Fig. 12b). This observation suggests that reducing the FSK spacing increases the interface shear resistance, thereby reducing end slip at a given deflection. This is because the greater the FSK spacing, the less composite action achieved, thus the larger the end slip. As the size of concrete slab increases, the end slip increases gradually (Fig. 12c and Fig. 12d). This is because increasing the size of concrete slab improves the flexural stiffness of specimens, which causes the curvature inconsistency between the concrete and FRP section and reduces their collaborative action.

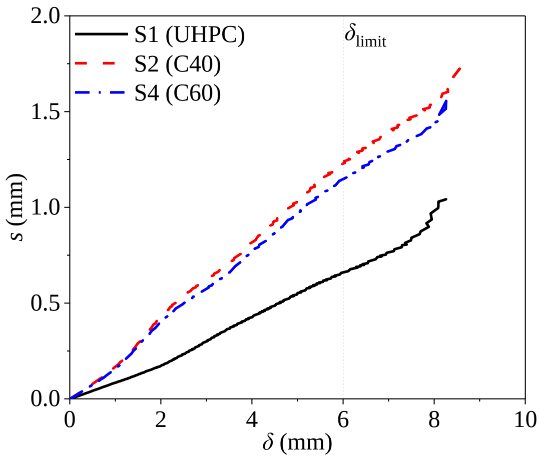

(a) Effect of concrete slab strength

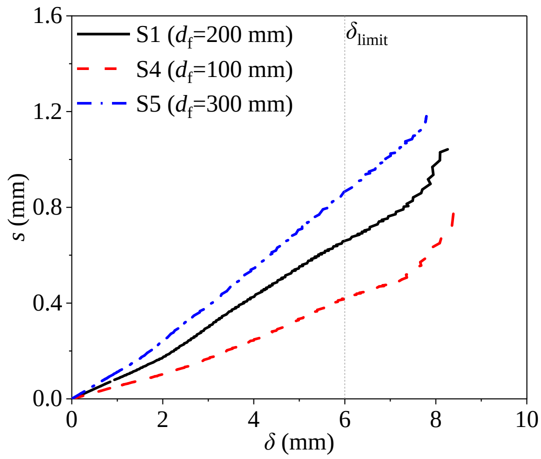

(b) Effect of FSK spacing

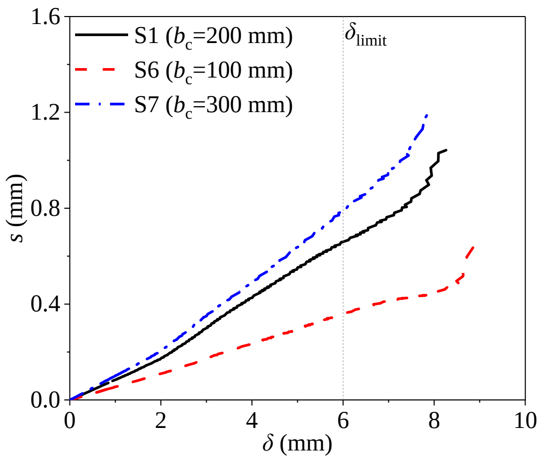

(c) Effect of concrete slab width

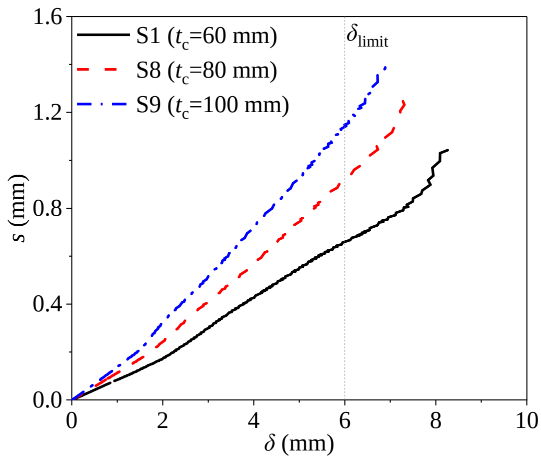

(d) Effect of concrete slab thickness

Fig. 12. Deflection-end slip strain curves.

4 Theoretical analysis

4.1 Shear capacity

The formulae for shear capacity of FRP-UHPC composite beams are established on the base of following assumptions. The interaction between the sectional shear force and bending moment can be ignored. The contribution of FRP profile flanges to shear performance is neglected. When the specimen reaches its ultimate shear capacity, the shear stress at FRP web is uniformly distributed along the height direction. The shear strain of web reaches its ultimate state at shear failure. Based on the assumptions, the shear capacity V_u is provided by both the FRP profile and UHPC slab, as presented by Eq. (2), where V_f and V_c are the shear resistance capacities of FRP profile and concrete, respectively.

$$V_u = V_c + V_f \tag{2}$$

The shear capacity of UHPC flexural members in a skewed cross-section can be calculated according to the code CECS 38-2004 [37], as shown in Eq. (3). Where, λ is the ratio of shear span to depth, f_t is the tensile strength of UHPC, and β_h is the effective thickness coefficient of concrete slab. The value of β_t = 1.0, $(800 / t_0)^{1/4}$ and 0.8, for t_0 < 800 mm, 800 < t_0 < 2000 mm, and t_0 > 2000 mm, respectively, where t_0 (= t_c) is the effective thickness of UHPC slab. β_v is the influential coefficient of steel fibers distributed in UHPC. For irregular steel fibers, β_v = 0.7, for bow-shaped steel fibers, β_v = 0.6, and for straight steel fibers, β_v = 0.5; λ_f (= $\rho_f l_f / d_f$) is the influence coefficient of steel fibers, where l_f, d_f, and ρ_f are the length, diameter and volume fraction of steel fibers, respectively.

$$V_c = 0.7\beta_h f_t b_c t_0 (1 + \beta_v \lambda_f) \tag{3}$$

The shear capacity of FRP web is given by Eq. (4), where A_w, G_{fw} and γ_{fw} are the cross-sectional area, shear modulus and shear strain of FRP web, respectively.

$$V_f = A_{fw} G_{fw} \gamma_{fw} \tag{4}$$

4.2 Deflection

4.2.1 Bending deformation

Since FRP primarily bear tensile stress while concrete slabs bear compressive stress, even if cracks occur in the concrete under normal service loads, the concrete in the cracked region has a limited effect on the overall stiffness and deflection of the composite beam. Therefore, it is reasonable to disregard the effects of concrete cracking during calculations, simplifying the analysis process and ensuring accurate and safe deflection predictions during the service stage. From the results tested, it can be observed that the load-deflection curve of the FRP-UHPC composite beams exhibits overall linearity under shear failure, and the interfacial slip is negligible. Therefore, in analyzing the bending deformation of composite beams experiencing shear failure, it is assumed that the bending deformation is the overall deformation of the combination of concrete slab and FRP profiles under full connection, while neglecting the reduction in bending stiffness due to the slip effect [15]. Based on the assumptions, the formula for bending deformation δ_f of FRP-UHPC composite beams under two-point loads is expressed by Eq. (5), where B is the flexural stiffness, P is the concentrated load applying on the specimen, L is the length of span, a is the length of shear span.

$$\delta_{\mathrm{f}} = \frac{Pa}{48B}\left(3L^2 - 4a^2\right) \tag{5}$$

The formula for flexural stiffness B is given by Eq. (6), where I is the inertia moment of the transformed section, I_0 is the sum of the inertia moment of FRP profiles and UHPC slab transformed by modulus of elasticity; I_f and I_c are the inertia moment of FRP profile and UHPC slab, respectively; E_f is the modulus of elasticity of FRP profile; A_0 is the sectional area transformed by modulus of elasticity, A_f and A_c are the sectional areas of FRP profile and UHPC slab; d_0 is the distance between the centroid of FRP profile and UHPC slab, and α_E is the ratio of elastic modulus of FRP to that of UHPC.

$$B = E_{\mathrm{f}} I \tag{6}$$

$$I = I_0 + A_0 d_0^{\,2} \tag{7}$$

$$I_0 = I_{\mathrm{f}} + I_{\mathrm{c}} / \alpha_{\mathrm{E}} \tag{8}$$

$$A_0 = A_{\mathrm{c}} A_{\mathrm{f}} / \left(\alpha_{\mathrm{E}} A_{\mathrm{f}} + A_{\mathrm{c}}\right) \tag{9}$$

4.2.2 Shear deformation

As the failure pattern of FRP-UHPC composite beams are shear failure, it is necessary to take the additional deformation caused by shear deformation into consideration. To simplify the analysis, it is assumed that the deformation of FRP flange occurs only in the plane and does not extend perpendicular to the neutral axis [38]. According to the Timoshenko beam theory, the shear deformation of specimens can be obtained by integrating along the length direction of the half-span, as presented in Eq. (10), where γ_{fw} and δ_s are the in-plane shear strain and deformation, respectively. G_{fw} is the shear modulus of FRP flange, V is the shear force applied on the element and τ is the corresponding shear stress.

$$\delta_s = \int_0^{2/L} \frac{V(x)}{G_{fw} A_{fw}} dx = \frac{V_f a}{2 G_{fw} A_{fw}} \tag{10}$$

Therefore, the total deformation δ_u can be obtained by adding the shear deformation δ_s to the bending deformation δ_f, as shown in Eq. (11).

$$\delta_u = \delta_f + \delta_s = \frac{Pa}{48B}\left(3L^2 - 4a^2\right) + \frac{V_f a}{2 G_{fw} A_{fw}} \tag{11}$$

4.3 Validation

The comparison between the predicted and experimental shear capacity V_u as well as their corresponding deflection δ_u is listed in Table 6. Since specimens S4 and S5 have the same mid-span section as S1 and only their FSK spacing differs, thus, only the results of S1 is presented here as the effect of FSK spacing on shear capacity is not considered. The subscripts "Exp" and "Cal" represent the experimental and calculated results, respectively, "Mean" and "CoV" represent the average value and coefficient of variation, respectively. The average value of the ratio of predicted to experimental shear capacities is 1.04, with a coefficient of variation of 0.09. Similarly, the average ratio of predicted to experimental deflections at the peak load is 1.03, with a coefficient of variation of 0.10. The predicted shear capacity of beams S2 and S3 (FRP-NSC composite beams) is lower than the experimental results due to the combined flexural and shear failure, whereas Eq. (2) only calculated the concrete shear capacity while ignoring the compression contribution of concrete. In all, the above calculation methods well predict the shear capacity and deflection. The composition of shear capacity and deflection of the specimens is illustrated in Fig. 13. In the case of FRP-UHPC composite beam, UHPC contributes to an average shear capacity accounting for 44%. On the other hand, for the FRP-NSC composite beam, NSC accounts for an average shear capacity of 20%. Therefore, when evaluating the shear capacity of FRP-UHPC composite beams, it is necessary to consider the contribution made by UHPC.

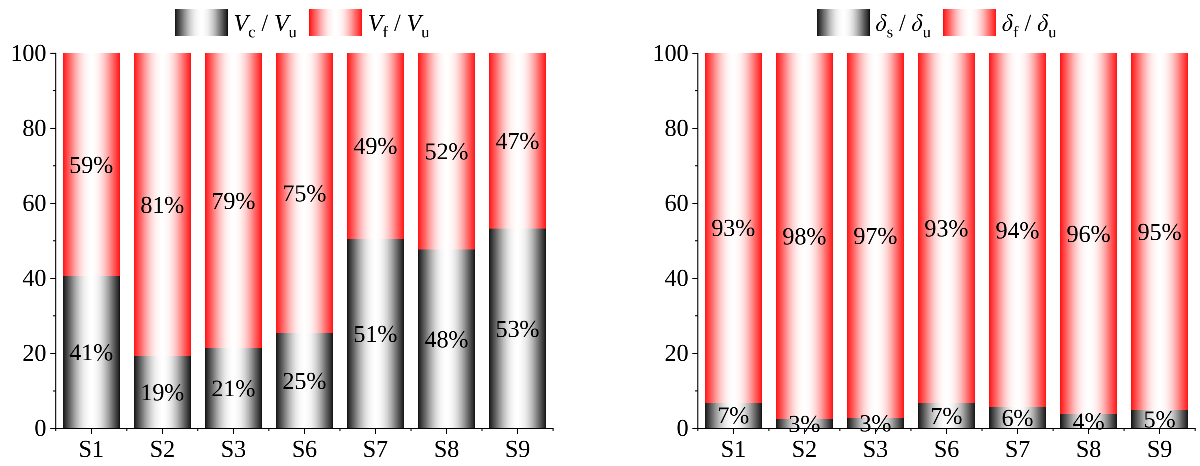

(a) Shear capacity (b) Deflection

Fig. 13. Composition of the shear capacity and deflection.

Tab. 6. Comparison of the predicted and experimental shear capacity and deflection.

No.	$V_{u,Exp}$ (kN)	$V_{u,Cal}$ (kN)	$V_{u,Exp}$ / $V_{u,Cal}$	$\delta_{u,Exp}$ (mm)	$\delta_{u,Cal}$ (mm)	$\delta_{u,Exp}$ / $\delta_{u,Cal}$
S1	168	168	1.00	8.26	8.20	1.01
S2	146	124	1.18	8.56	7.26	1.18
S3	149	133	1.12	8.27	7.30	1.13
S6	162	146	1.11	8.88	7.90	1.12
S7	172	193	0.89	8.06	8.71	0.92
S8	190	191	0.99	7.39	7.97	0.93
S9	218	214	1.02	6.92	7.68	0.90
Mean			1.04			1.03
CoV			0.09			0.10

5 Conclusions

Four-point flexural testing was carried out on FRP-UHPC composite beams enhanced by FSK to investigate the effects of strength of concrete, spacing of FSK, width and thickness of concrete slab.

(1) The failure mode of FRP-UHPC composite beams enhanced by FSK is mainly attributed to shear, whereas FRP-NSC composite beams typically exhibit flexural-shear synergistic failure. Both types of beams demonstrate linear-elastic behavior in their load-deflection curves prior to concrete cracking. However, after cracking occurs, FRP-UHPC beams maintain a near-linear progression until failure, while FRP-NSC beams display a nonlinear response.

(2) Prior to failure, the mid-span distribution of longitudinal strain along the sectional height direction tends to follow a linear pattern, which is basically fit the plane-section assumption. However, upon reaching ultimate load, a noticeable interface slip occurs between the bottom of concrete slab and upper flange of FRP profile.

(3) In elastic stage, the compressive strain on the top of UHPC slab and tensile strain on the bottom flange of FRP profile are uniformly distributed; when moving into the elastic-plastic stage, the strain is no longer uniform for the shear lag effect. And the shear lag effect becomes more evident with the increase of concrete slab width.

(4) Using UHPC slab, decreasing the spacing of FSK, and increasing the size of concrete slab can effectively improving the shear performance and reduce interface slip of composite beams. Due to the limited shear strength of FRP, the strong compressive performance of UHPC cannot be fully utilized, and the deflection is determined by shear failure. It is necessary to increase the thickness of web or provide local reinforcement to enhance the shear performance.

(5) Based on the reasonable assumptions, the formulae for shear capacity and deflection of FRP-UHPC composite beams considering shear deformation is proposed. The predicted results coincide well with the test results.

Overall, the FRP-concrete composite beams enhanced by FSKs designed in this study exhibited good interfacial bonding performance, and their shear performance was sufficient under serviceability limit state. Although the use of UHPC instead of NSC improved the initial stiffness and shear capacity of the composite beams to some extent, the improvement was not significant. Given the high cost of UHPC, the FRP-UHPC composite beams showed poor cost-effectiveness. Therefore, future research should focus on enhancing the shear performance of FRP web to fully leverage the superior mechanical properties of UHPC.

Acknowledgement

The authors would like to acknowledge the financial support to the work by the High-End Foreign Experts Project of Ministry of Science and Technology, China (G2022014054L), the Science and Technology Cooperation Fund Project of Yangzhou City and University (YZ2022194), the Science and Technology Project of Jiangsu Construction System (2023ZD104 and 2023ZD105), the Yangzhou Construction System Science and Technology Project (202309 and 202312), and the Research Project of Jiangsu Civil Engineering and Architecture Society (the Second Half of 2022), Graduate Research and Innovation Projects of Jiangsu Province (KYCX24_3750), Jiangsu Provincial Government Scholarship for Studying Abroad (2024), Excellent Doctoral Dissertation Fund of Yangzhou University (2024).

Credit authorship contribution statement

Zhiwen Zhang: Investigation, Software, Writing-Original draft, Review and Editing. Ashraf Ashour: Formal analysis, Supervision, Writing-Review and Editing. Wenjie Ge: Conceptualization, Methodology, Funding, Formal analysis, Writing – Review and Editing.

Declaration of Competing Interest

The authors declare that they have no known competing financial interests or personal relationships that could have appeared to influence the work reported in this paper.

Data availability statement

Data will be made available on request.

Reference

[1] H. Zhou, S. Chen, Y. Du, Z. Lin, X. Liang, J. Liu, F. Xing, Field test of a reinforced concrete bridge under marine environmental corrosion, Eng. Fail. Anal. 115 (2020) 104669.

[2] C. Su, X. Wang, L. Ding, et al. Effect of carbon nanotubes and silica nanoparticles on the

durability of basalt fiber reinforced polymer composites in seawater and sea sand concrete environment [J]. Polym Composite. 42 (2021).

[3] X. Zhang, X. Wang, X. Liang, et al. Experimental study on the durability of polymer-impregnated basalt textile applied as concrete reinforcement [J]. Polym Composite. 43 (6) (2022).

[4] Z.Q. Dong, T.H. Han, B. Zhang, H. Zhu, G. Wu, Y. Wei, P. Zhang, A review of the research and application progress of new types of concrete-filled FRP tubular members. Constr. Build. Mater. 312 (2021) 125353.

[5] Z. Wu, W. Li, N. Sakuma, Innovative externally bonded FRP/concrete hybrid flexural members, Compos. Struct. 72 (3) (2006) 289-300.

[6] H. Nguyen, H. Mutsuyoshi, W. Zatar, Hybrid FRP-UHPFRC composite girders: Part 1-Experimental and numerical approach, Compo. Struct. 125 (2015) 631-652.

[7] T. Liu, P. Feng, X. Lu, J. Q. Yang, Y. Wu, Flexural behavior of novel hybrid multicell GFRP-concrete beam, Compos. Struct. 250 (2020) 112606.

[8] C. Eamon, N. Grace, X. Shi, E. Jensen, Life-cycle cost analysis of carbon fiber-reinforced polymer reinforced concrete bridges, ACI Struct. J. 109 (5) (2012) 697-704.

[9] X.X. Zou, H.W. Lin, P. Feng, Y. Bao, J.Q. Wang, A review on FRP-concrete hybrid sections for bridge applications, Compos. Struct. 262 (2021) 113336.

[10] J.Q. Wang, S.L. Li, Z.T. Lv, Calculation and experiments on ultimate bearing capacity of FRP-concrete composite beams based on single layer failure criteria, J. southeast univ. 43 (5) (2013) 952-956. (in Chinese)

[11] C. A. Neagoe, L. Gil, M.A. Pérez, Experimental study of GFRP-concrete hybrid beams with low degree of shear connection, Constr. Build. Mater. 101 (2015) 141-151.

[12] X.X. Zou, J. Chen, H. Jiang, J.Q. Wang, High shear strength post-forming FRP profiles: manufacture and testing, China Civil Eng. J. 49 (4) (2016) 40-47. (in Chinese)

[13] C.A. Neagoe, L. Gil, Analytical procedure for the design of PFRP-RC hybrid beams including shear interaction effects, Compo. Struct. 132 (2015) 122-135.

[14] M.A. Al-Ramahee, T. Chan, K.R. Mackie, et al. Lightweight UHPC-FRP Composite Deck System, J. Bridge Eng. 22 (7) (2017) 404-412.

[15] P. Zhang, X.L. Lv, Y. Liu, X.X. Zou, Y.Z. Li, J.Q. Wang, S.A. Sheikh, Novel fiber reinforced polymers (FRP)-ultrahigh performance concrete (UHPC) hybrid beams with improved shear

performance, Constr. Build. Mater. 286 (2021) 122720.

[16] P. Richard, M. Cheyrezy. Composition of reactive powder concretes, Cement Concrete Res. 25 (7) (1995) 1501-1511.

[17] N.M. Azmee, N. Shafiq, Ultra-high performance concrete: From fundamental to applications, Case Stu. Constr. Mat. 9 (2018) e00197.

[18] Y.Z. Lin, J.C. Yan, Z.F. Wang, C.Y. Zou, Effects of steel fibers on failure mechanism of S-UHPC composite beams applied in the Arctic offshore structure, Ocean Engineering, 234 (2021) 109302.

[19] X.X. Zou, J.Q. Wang. Experimental study on joints and flexural behavior of FRP truss-UHPC hybrid bridge, Compos. Struct. 203 (2018) 414-424.

[20] T. Siwowski, M. Rajchel, Structural performance of a hybrid FRP composite-lightweight concrete bridge girder, Compos. B Eng. 174 (2019) 107055.

[21] Specification for mix proportion design of ordinary concrete JGJ 55-2019. Beijing, China; 2019.

[22] Reactive Powder Concrete GB/T 31387−2015. Beijing, China; 2015.

[23] Standard for test methods of concrete physical and mechanical properties GB/T 50081-2019. Beijing, China; 2019.

[24] T/CBMF 37−2018, T/CCPA 7−2018, Fundamental characteristics and test methods of ultra-high performance concrete. Beijing, China; 2018.

[25] W.Z. Zheng, L. Li, Y. Wang, Compressive stress-strain relationship of steel fiber-reinforced reactive powder concrete after exposure to elevated temperatures, Constr. Build. Mater. 35 (2012) 931-940.

[26] ASTM D3039/D3039M-14, Standard test method for tensile properties of polymer matrix composite materials. American: American Society for Testing Materials, 2014.

[27] GB/T 1448-2005, Fiber-reinforced plastics composites-Determination of compressive properties. China, 2005.

[28] ASTM D3518/D3518M-18, Standard test method for in-plane shear response of polymer matrix composite materials by tensile test of a ±45° laminate. American: American Society for Testing Materials, 2018.

[29] JGJ 138-2016, Code for design of composite structures. China; 2016.

[30] N. Deskovic, U. Meier, T.C. Triantafillou, Innovative design of FRP combined with concrete:

long-term behavior, J. Struct. Eng. 121 (7) (1995) 1079-89.

[31] P. Zhang, H. Liu, D.Y. Gao, J. Zhao, H. Feng, G.B. Tang, Shear-bond behavior of the interface between FRP profile and concrete by the double-lap push shear method, J. Compos. Constr. 21 (4) (2017) 04017012.

[32] W.J. Ge, Z.W. Zhang, Z.W. Guan, A. Ashour, Y. Ge, Y.W. Chen, H.B. Jiang, C.Z. Sun, S. Yao, W.H. Yan, D.F. Cao, Numerical study on flexural and bond-slip behaviours of GFRP profiled-concrete composite beams with groove shear connector, Eng. Struct. 275 (2023) 115226.

[33] X.D. Zhao, X.D. Shao, J.H. Cao, Z.X Shao, R.J. Ying-Li, Experimental studies on shear behavior of steel-UHPC composite beam with hot rolled shape steel, Eng. Struct. 274 (2023) 115160.

[34] S.H. He, G. Yang, W.J. Zhou, Q.F. Li, Y. Dong, Evaluation of shear lag effect in HSS-UHPC composite beams with perfobond strip connectors: Experimental and numerical studies, J. Constr. Steel Res. 194 (2022) 107312.

[35] A. KOZMA, A. M. G. COELHO, J. YANG, C. Odenbreit. A new concept and algorithm to transfer brittle and arbitrary load-slip curves into an effective shear resistance suitable for Eurocode 4 [J]. J Theor App Mech-Pol, 60 (4) (2022) 705-718.

[36] X.Z. Lu, J.G. Teng, L.P. Ye, J.J. Jiang, Bond-slip models for FRP sheets/plates bonded to concrete, Eng. Struct. 27(6) 2005, 920-937.

[37] CECS 38: 2004, Technical specification for fiber reinforced concrete structures. China, 2004.

[38] X.X. Zou, P. Feng, Y. Bao, J.Q. Wang, H.H. Xin, Experimental and analytical studies on shear behaviors of FRP-concrete composite sections, Eng. Struct. 215 (2020) 110649.